A nine-dimensional Lorenz system to study high-dimensional chaos

To cite this article: Peter Reiterer *et al* 1998 *J. Phys. A: Math. Gen.* **31** 7121

View the article online for updates and enhancements.

A nine-dimensional Lorenz system to study high-dimensional chaos

Peter Reiterer†, Claudia Lainscsek†, Ferdinand Schürrer†, Christophe Letellier‡ and Jean Maquet‡

† Institute for Theoretical Physics, Technical University of Graz, Petersgasse 16, A-8010 Graz, Austria
‡ LESP/UMR 6614—CORIA, Université de Rouen, Place Emile Blondel, 76131 Mont Saint-Aignan Cedex, France

Abstract. We examine the dynamics of three-dimensional cells with square planform in dissipative Rayleigh–Bénard convection. By applying a triple Fourier series ansatz up to second order, we obtain a system of nine nonlinear ordinary differential equations from the governing hydrodynamic equations. Depending on two control parameters, namely the Rayleigh number and the Prandtl number, the asymptotic behaviour can be stationary, periodic, quasiperiodic or chaotic. A period-doubling cascade is identified as a route to chaos. Hereafter, the asymptotic behaviour progressively evolves towards a hyperchaotic attractor. For given values of control parameters beyond the accumulation point, we observe a low-dimensional chaotic attractor as is currently done for dissipative systems. Although the correlation dimension strongly suggests that this attractor could be embedded in a three-dimensional space, a topological characterization reveals that a higher-dimensional space must be used. Thus, we reconstruct a four-dimensional model which is found to be in agreement with the properties of the original dynamics. The nine-dimensional Lorenz model could therefore play a significant role in developing tools to characterize chaotic attractors embedded in phase space with a dimension greater than 3.

1. Introduction

It is now well known that chaotic dynamics may be generated by many kinds of experiments from various fields of science such as hydrodynamics, astrophysics, chemistry, biology, electronics, etc. It is therefore of particular interest to possess an extended tool box to characterize the dynamics of the studied physical systems. From the pioneering paper by Lorenz [1], many analyses have been developed which may be separated into two classes.

First, the geometrical properties of attractors on which the asymptotic motion settles down have been investigated. Such methods are based on a notion of distance in the reconstructed phase space according to Packard *et al* [2] and the very mathematical paper by Takens [3]. Geometrical properties present the attractive feature of being usable in a *n*-dimensional space. For instance, the correlation dimension [4] and Lyapunov exponents [5] have been commonly used to characterize attractors. The knowledge of Lyapunov exponents gives an indication about the predictability of a system and also about the number of active dynamical degrees of freedom involved in it [6, 7]. Nevertheless, the computation of such geometrical quantities is very sensitive to noise perturbations and not very useful in identifying different classes of systems.

A second approach based on the population of periodic orbits which constitutes the skeleton of the attractor allows us to quantify how the chaotic behaviour develops. In particular, a partition of the attractor induces an identification of each orbit by a symbolic sequence [8, 9]. This encoding, called the symbolic dynamics, allows us to predict a theoretical order of creation of periodic orbits under the change of a control parameter [10].

In the early 1990s, the idea arose that topological properties could complement the characterization of geometrical properties. Indeed, it has been demonstrated that the relative organization of periodic orbits provides a fine characterization of an attractor [11–13]. The topological characterization is based on topological invariants, namely linking numbers which are robust under control parameter changes. Associated with the use of symbolic dynamics it constitutes a powerful tool to study attractors. In particular, it is robust with respect to noise perturbations since it essentially involves the low periodic orbits which are not really affected by noise. Unfortunately, such a characterization is nowadays restricted to three-dimensional spaces.

It is therefore an important task to develop such a characterization in higher-dimensional spaces. The topological characterization is based on the knot theory which states that all knots—a periodic orbit is a knot—are trivial in four-dimensional (4D) spaces. Typical invariants are then useless, and it is important to find extended versions of them or new ones for higher-dimensional phase spaces. In order to try to extend the understanding of the dynamical structure of high-dimensional systems, two approaches can be used. First, one may develop new tools from a theoretical approach and, consequently, must have a large mathematical background. Second, one may try to understand how adding degrees of freedom to a dynamical system can affect its dynamical structure. For this latter approach, the first step is to consider a dynamical system whose dimension is greater than 3 and generates an asymptotic behaviour which is not so far from the well-documented three-dimensional (3D) attractors. Indeed, many high-dimensional systems exist, but they usually present very complex dynamics which do not provide useful test cases in the understanding of the high-dimensional dynamical structure. A typical example is the 4D system proposed by Rössler [14] which generates hyperchaotic motion.

Our goal is therefore to derive a high-dimensional system generating asymptotic behaviour similar to typical attractors exhibited by 3D systems such as the Rössler system [15] or the Lorenz system [1]. A nine-dimensional (9D) model is derived by applying a triple Fourier expansion to the Boussinesq–Oberbeck equations governing thermal convection in a 3D spatial domain by using an approach similar to Lorenz's.

We consider a horizontal layer of fluid, heated uniformly from below and cooled from above. Due to thermal expansion, a density gradient opposite to the direction of gravity arises. The resulting model is constituted by a system of nine ordinary differential equations (ODEs) which generate a period-doubling cascade as a route to chaos. The strong truncation of the system of modes prevents any relationship of its solutions with experimental observations except in the case of Rayleigh numbers close to the critical value as observed in the Lorenz model. In this paper, we show that the asymptotic motion settles down on a chaotic attractor whose correlation dimension is approximately 2.08. We then reconstruct a 3D model from one of the nine dynamical variables which confirms that a large part of the dynamics may be captured in a 3D phase space. However, a topological characterization achieved in a 3D subspace shows that a higher-dimensional phase space is required to describe the underlying dynamics completely. Thus we reconstruct a 4D model which is found to be in agreement with the original dynamics.

This paper is organized as follows. In section 2 the 9D Lorenz model is derived from the Boussinesq–Oberbeck equations. Section 3 is devoted to the dynamical analysis of the

9D system by using a geometrical approach, i.e. computation of the correlation dimension, as well as a global vector field reconstruction starting from either a scalar time series or a topological characterization.

2. The governing equations describing square convection cells

We consider a viscous fluid layer of infinite-horizontal extent that is uniformly heated from below. Let t and $\boldsymbol{x}$, respectively, be the time and space variables. The density field $\rho(\boldsymbol{x}, t)$ describes the mass distribution of the fluid. The physical state is determined by the pressure $p(\boldsymbol{x}, t)$, the temperature $T(\boldsymbol{x}, t)$ and the velocity field $\boldsymbol{v}(\boldsymbol{x}, t)$.

We will employ the Boussinesq–Oberbeck approximation in order to simplify the mathematical analysis. This means that ρ is considered to be constant except when it modifies the gravity term. In this term, the density is assumed to be independent of the pressure and a linear function of the temperature. The vertical density variation actually provides the driving mechanism of the convective motions. Furthermore, we assume that all material properties are constant. An extensive discussion of this set of approximations can be found in Cordon and Velarde [16].

Then the dynamical behaviour of the medium is governed by three nonlinear partial differential equations (PDEs) [17, 18], namely the equation of continuity

$$\operatorname{div} \boldsymbol{v} = 0 \tag{1}$$

that corresponds to preservation of mass, the Navier–Stokes equation

$$\frac{\partial \boldsymbol{v}}{\partial t} + (\boldsymbol{v} \cdot \nabla)\boldsymbol{v} = \frac{\rho}{\rho_0}\boldsymbol{g} - \frac{1}{\rho_0}\nabla p + \nu\nabla^2\boldsymbol{v} \tag{2}$$

that corresponds to preservation of momentum, and the equation of thermal conductivity

$$\frac{\partial T}{\partial t} + (\boldsymbol{v} \cdot \nabla)T = \chi\nabla^2 T \tag{3}$$

that corresponds to the preservation of energy. Here $\boldsymbol{g} = (0, 0, -g)$ denotes the vector of gravity, ρ_0 standard density, ν kinematic viscosity and χ thermal conductivity. Note that we write ∇^2 for the Laplacian.

Let T_0 be the temperature at the upper boundary. By introducing the coefficient of volume expansion $\alpha = -(1/\rho)(\partial\rho/\partial T)_p$, ρ can be written approximately as

$$\rho(T) = \rho_0[1 - \alpha(T - T_0)].$$

In the case of no convection, the temperature profile linearly decreases with height. If convection occurs we are interested in the deviation from the linear temperature profile which will be denoted by θ. We can express T by means of θ as

$$T(x, y, z, t) = T_0 + \Delta T\left(1 - \frac{z}{h}\right) + \theta(x, y, z, t). \tag{4}$$

Here ΔT is the temperature difference between the lower and upper boundaries, h is the depth of the fluid layer, and z denotes the vertical coordinate of $\boldsymbol{x}$ measured positive upwards with $z = 0$ corresponding to the lower boundary and $z = h$ corresponding to the upper boundary. Since the temperature at $z = 0$ is higher than the temperature at $z = h$, ΔT is greater than zero. The horizontal coordinates are x and y.

Now we introduce dimensionless variables

$$\boldsymbol{x} \rightarrow \frac{h}{\pi}\boldsymbol{x} \qquad t \rightarrow \frac{h^2}{\pi^2\chi}t \qquad \theta \rightarrow \frac{\pi^3\chi\nu}{g\alpha h^3}\theta$$

and take the curl of (2) to eliminate p. This yields the following system

$$\text{div } v = 0 \tag{5}$$

$$\frac{\partial \omega}{\partial t} - \text{curl}(v \times \omega) = \sigma \text{ curl}(\theta e_z) + \sigma \nabla^2 \omega \tag{6}$$

$$\frac{\partial \theta}{\partial t} + (v \cdot \nabla)\theta = \nabla^2 \theta + Rw. \tag{7}$$

Here $\omega = \text{curl } v$ is the vorticity field, e_z is the unit vector in the vertical direction and w is the vertical component of v. For further reading u and v denote the horizontal components of v.

The Prandtl number

$$\sigma = \frac{\nu}{\chi}$$

is a measure of the relative importance of momentum vorticity diffusion to heat conduction by molecular collisions.

The Rayleigh number

$$R = \frac{\alpha g \Delta T h^3}{\pi^4 \nu \chi}$$

is a non-dimensional measure of the vertical temperature difference. It gives the ratio of free energy liberated by buoyancy to the energy dissipated by heat and viscous drag.

Next we have to consider boundary conditions. The horizontal boundaries are either rigid walls or free surfaces. We will only deal with free surfaces which means that both the normal stress as well as the shearing stress are zero. That leads to $u_z = v_z = 0$. From (5) vanishing shearing stress leads to $w_{zz} = 0$. Additionally, w must vanish at the boundaries. Since the boundaries are assumed to be perfect heat conductors, θ must also vanish at the boundaries because of (4).

In summary, the boundary conditions for free surfaces are then

$$w|_{z=0,\pi} = w_{zz}|_{z=0,\pi} = u_z|_{z=0,\pi} = v_z|_{z=0,\pi} = \theta|_{z=0,\pi} = 0. \tag{8}$$

Rayleigh [19] neglected the nonlinear terms $(v \cdot \nabla)v$ and $(v \cdot \nabla)\theta$ in (2) and (3) and showed that the onset of convection occurs at a Rayleigh number

$$R_0(k) = \frac{(1 + k^2)^3}{k^2} \tag{9}$$

which is independent of σ. The wavenumber k obeys the relation

$$k^2 = k_x^2 + k_y^2 \tag{10}$$

where k_x and k_y denote the wavenumbers in the horizontal directions. The minimum of (9) is the so-called critical Rayleigh number given by

$$R_c = \frac{27}{4}.$$

The critical wavenumber

$$k_c = \frac{1}{\sqrt{2}} \tag{11}$$

is the value of k where the minimum of the graph $R_0(k)$ occurs.

For values of R less than R_c the fluid is at rest and no convection takes place. For $R = R_c$ the state of conduction is marginally unstable and a convective motion with wavenumber k_c is set up. The entire fluid layer should change spontaneously from the state of rest to cellular convective motion, if the temperatures on the top and bottom surfaces of

the layer are indeed uniform. It is a well known fact that at the onset of convection, the linearized versions of the governing equations (1)–(3) possess a degeneracy—no cell shape is preferred to any other [20, 21].

In order to examine the full system of nonlinear PDEs, Lorenz expanded equations (1)–(3) in double Fourier series [1]. The resulting system of equations was then truncated radically. He obtained a system of three nonlinear ODEs, the so-called Lorenz equations, to describe two-dimensional rolls. It is known that this approach reflects the dynamics in the PDEs only for $r = 1 + \mathcal{O}(\epsilon^2)$ (cf equation (19)), where $\epsilon \ll 1$ is the amplitude of motion [21].

As we are interested in derivating a higher-dimensional model corresponding to the description of three-dimensional square convection cells we extend Lorenz's approach to a triple Fourier series ansatz. By introducing a vector potential $\boldsymbol{A}$, $\boldsymbol{v}$ can be represented as

$$\boldsymbol{v} = \operatorname{curl} \boldsymbol{A} \tag{12}$$

in accordance with (5). In order to describe square cells we set

$$k_x = k_y = a \tag{13}$$

and expand θ and the components A_1, A_2, A_3 of $\boldsymbol{A}$ in triple Fourier series with the Fourier coefficients $\Theta^{ij\ell}$, $A_1^{ij\ell}$, $A_2^{ij\ell}$ and $A_3^{ij\ell}$ functions of t alone

$$A_1(\boldsymbol{x}, t) = \sum_{i=0}^{\infty} \sum_{j=1}^{\infty} \sum_{\ell=1}^{\infty} \cos(iax) \sin(jay) \sin(\ell z) A_1^{ij\ell}(t) \tag{14a}$$

$$A_2(\boldsymbol{x}, t) = \sum_{i=1}^{\infty} \sum_{j=0}^{\infty} \sum_{\ell=1}^{\infty} \sin(iax) \cos(jay) \sin(\ell z) A_2^{ij\ell}(t) \tag{14b}$$

$$A_3(\boldsymbol{x}, t) = \sum_{i=1}^{\infty} \sum_{j=1}^{\infty} \sum_{\ell=0}^{\infty} \sin(iax) \sin(jay) \cos(\ell z) A_3^{ij\ell}(t) \tag{14c}$$

$$\theta(\boldsymbol{x}, t) = \sum_{i=0}^{\infty} \sum_{j=0}^{\infty} \sum_{\ell=1}^{\infty} \cos(iax) \cos(jay) \sin(\ell z) \Theta^{ij\ell}(t). \tag{15}$$

With (12) this leads to the following expressions for the components of $\boldsymbol{v}$

$$u(\boldsymbol{x}, t) = \sum_{i=1}^{\infty} \sum_{j=0}^{\infty} \sum_{\ell=0}^{\infty} \sin(iax) \cos(jay) \cos(\ell z) [ja A_3^{ij\ell}(t) - \ell A_2^{ij\ell}(t)] \tag{16a}$$

$$v(\boldsymbol{x}, t) = \sum_{i=0}^{\infty} \sum_{j=1}^{\infty} \sum_{\ell=0}^{\infty} \cos(iax) \sin(jay) \cos(\ell z) [\ell A_1^{ij\ell}(t) - ia A_3^{ij\ell}(t)] \tag{16b}$$

$$w(\boldsymbol{x}, t) = \sum_{i=0}^{\infty} \sum_{j=0}^{\infty} \sum_{\ell=1}^{\infty} \cos(iax) \cos(jay) \sin(\ell z) [ia A_2^{ij\ell}(t) - \ell a A_1^{ij\ell}(t)]. \tag{16c}$$

It can easily be shown that equations (15)–(16c) satisfy the boundary conditions (8).

When looking for the simplest nonlinear model, we selected, by trial and error, only very certain terms of the Fourier mode expansions, namely A_1^{022}, A_1^{111}, A_2^{202}, A_2^{111}, A_3^{220}, Θ^{002}, Θ^{022}, Θ^{202} and Θ^{111}. For this task, Stephen Wolfram's Mathematica was a great help to us. Next we introduce for convenience time $t' := (1 + 2a^2) t$ and the vector

$$C(t') := \{C_1, \ldots, C_9\} = \{A_1^{022}, A_1^{111}, A_2^{202}, A_2^{111}, A_3^{220}, \Theta^{002}, \Theta^{022}, \Theta^{202}, \Theta^{111}\}.$$

By neglecting all trigonometric terms of third order and higher, the ansatz

$$A_1 = \frac{1 + 2a^2}{a} \sin(2ay) \sin(2z) C_1 + \frac{2\sqrt{2}\left(1 + 2a^2\right)}{a} \cos(ax) \sin(ay) \sin(z) C_2$$

$$A_2 = \frac{1 + 2a^2}{a} \sin(2ax) \sin(2z) C_3 + \frac{2\sqrt{2}\left(1 + 2a^2\right)}{a} \sin(ax) \cos(ay) \sin(z) C_4$$

$$A_3 = \frac{1 + 2a^2}{a^2} \sin(2ax) \sin(2ay) C_5 \tag{17}$$

$$\theta = \frac{\left(1 + 2a^2\right)^3}{a^2} \cos(2ay) \sin(2z) C_7 + \frac{\left(1 + 2a^2\right)^3}{a^2} \cos(2ax) \sin(2z) C_8$$

$$+ \frac{\left(1 + 2a^2\right)^3}{a^2} \sin(2z) C_6 + \frac{\sqrt{2}\left(1 + 2a^2\right)^3}{a^2} \cos(ax) \cos(ay) \sin(z) C_9$$

yields a system of 10 ODEs for the nine variables C_i. Since one of these 10 equations depends linearly on two others, it can be omitted and we finally obtain the following system of nine nonlinear ODEs:

$$\dot{C}_1 = -\sigma b_1 C_1 - C_2 C_4 + b_4 C_4{}^2 + b_3 C_3 C_5 - \sigma b_2 C_7$$

$$\dot{C}_2 = -\sigma C_2 + C_1 C_4 - C_2 C_5 + C_4 C_5 - \sigma C_9/2$$

$$\dot{C}_3 = -\sigma b_1 C_3 + C_2 C_4 - b_4 C_2{}^2 - b_3 C_1 C_5 + \sigma b_2 C_8$$

$$\dot{C}_4 = -\sigma C_4 - C_2 C_3 - C_2 C_5 + C_4 C_5 + \sigma C_9/2$$

$$\dot{C}_5 = -\sigma b_5 C_5 + C_2{}^2/2 - C_4{}^2/2 \tag{18}$$

$$\dot{C}_6 = -b_6 C_6 + C_2 C_9 - C_4 C_9$$

$$\dot{C}_7 = -b_1 C_7 - r C_1 + 2 C_5 C_8 - C_4 C_9$$

$$\dot{C}_8 = -b_1 C_8 + r C_3 - 2 C_5 C_7 + C_2 C_9$$

$$\dot{C}_9 = -C_9 - r C_2 + r C_4 - 2 C_2 C_6 + 2 C_4 C_6 + C_4 C_7 - C_2 C_8.$$

This system is self-consistent in the sense that no further Fourier modes appear and no algebraic equations which relate the variables C_i arise when (17) is inserted into (5)–(7). With $\dot{C}_i$ we denote the derivative of C_i with respect to t', and r, the reduced Rayleigh number, is the quotient

$$r = \frac{R}{R_c}. \tag{19}$$

The constant parameters b_i, a measure for the geometry of the square cell, is defined by

$$b_1 := 4\frac{1 + a^2}{1 + 2a^2} \qquad b_2 := \frac{1 + 2a^2}{2\left(1 + a^2\right)} \qquad b_3 := 2\frac{1 - a^2}{1 + a^2}$$

$$b_4 := \frac{a^2}{1 + a^2} \qquad b_5 := \frac{8a^2}{1 + 2a^2} \qquad b_6 := \frac{4}{1 + 2a^2}.$$

In the remaining part of this paper we will drop the prime of t' and will simply write t. In order to fulfil (10), (11) and (13), we set $a = \frac{1}{2}$ for the wavenumber in the horizontal direction.

3. Dynamical analysis

3.1. Geometrical approach

In order to exemplify typical behaviour which may be observed in this 9D model, we fix the value of σ to be equal to 0.5 and the reduced Rayleigh number r is varied. For values of r less than 1, the trivial fixed point defined by $v = 0$ and $\theta = 0$ is stable and the fluid is at rest. At $r = 1$, the trivial fixed point $C^* = 0$ becomes unstable, and a new equilibrium is established which is characterized by a stationary convective flow. It has been observed that such an evolution is generated for all values of the Prandtl number σ while the bifurcation diagram for values of r greater than 1 strongly depends on σ. For $\sigma = 0.5$ and $r = r_H \approx 13.07$, a limit cycle is born by a Hopf bifurcation and the convective motion becomes time dependent. In the range $[r_H, r_\infty]$, with $r_\infty = 14.17$, there is a period-doubling cascade. Such a behaviour is rather interesting since this route is very well documented, and it is known that the chaotic regime observed beyond the accumulation point r_∞ belongs to the universal class exhibited by Feigenbaum [23] or, independently, Coullet and Tresser [24]. This means that the chaotic attractor is expected to be low dimensional and characterized by a first-return map with a differentiable maximum, namely a unimodal map. When such a chaotic regime was studied by using topological characterization or symbolic dynamics [12, 13, 25, 26], it was always for systems whose attractor can be embedded in a 3D phase space. It is therefore of great interest to study how a period-doubling cascade generated by a higher-dimensional system is organized, as seen in the model derived by Franceschini and Tebaldi [27] or in our 9D Lorenz model.

Due to the dissipative nature of the 9D Lorenz model, the dynamics of the system for $r = 14.22$ settles down on a chaotic attractor which may be embedded in a space whose dimension d_E is smaller than 9. Such an embedding dimension d_E may be equal to the first integer larger than the correlation dimension D_K defined as

$$D_K = \lim_{N \to \infty} \lim_{\rho \to 0} \frac{\log_2 C(\rho)}{\log_2 \rho}$$

where $C(\rho)$ is the correlation integral [4] and N is the overall number of data points. The correlation dimension D_K measures the number of points y_j which are correlated with each other on a sphere with radius ρ around the randomly chosen N_{ref} reference points y_i. The correlation integral $C(\rho)$ reads as

$$C(\rho) = \frac{1}{N_{\text{ref}}} \frac{1}{N} \sum_{i=1}^{N_{\text{ref}}} \sum_{j=1}^{N} H(\rho - |y_i - y_j|)$$

where $H(y)$ is the Heaviside function defined by

$$H(y) = \begin{cases} 0 & (y \leqslant 0) \\ 1 & (y > 0) \end{cases}$$

and $|y_i - y_j|$ is the Euclidean norm.

The correlation dimension has been estimated for the control parameter values $\sigma = 0.5$ and $r = 14.22$ (figure 1). It has been computed for the attractor embedded in the 9D phase space as well as for the attractor reconstructed by using the delay coordinates [2] starting from the C_5-variable. In both cases, the correlation dimension D_K is obtained from the slope of the $\log_2 C(\rho)$ versus $\log_2(\rho)$ plot by applying a Savitzky–Golay filter of fourth order [28]. From the plateau, we estimate the dimension to be approximately 2.08 in both cases, which strongly suggests that the dynamical analysis may be performed in a 3D phase
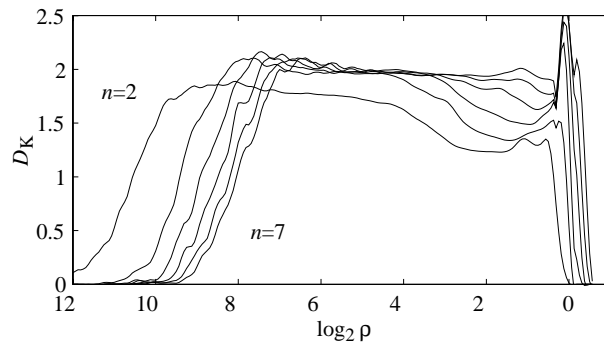
Figure 1. Correlation dimension D_K for the attractor reconstructed from the C_5-time series. The system parameters are $r = 14.22$ and $\sigma = 0.5$. The correlation dimension D_K is computed in spaces spanned by delay coordinates whose dimension n varies from 2 up to 7. The time delay $\tau = 0.97$ is selected by taking the first minimum of the mutual information.
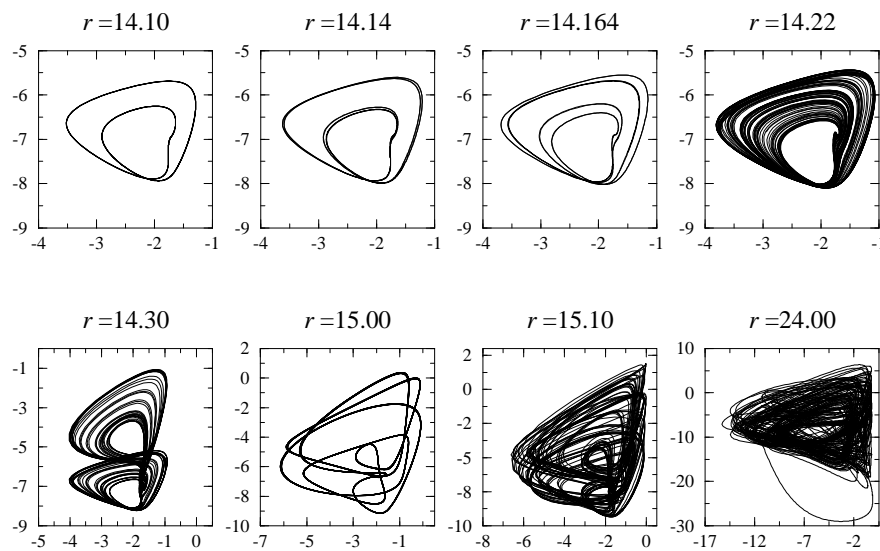

Figure 2. Phase space projections of the 9D attractor on the C_6–C_7 plane for $\sigma = 0.5$ and increasing r. Initial conditions correspond to the state vector $C^{(0)} = \{0.01, 0, 0.01, 0, 0, 0, 0, 0, 0.01\}$. The timestep δt is equal to 0.05 except for $r = 24.0$ where it is equal to 0.01.

space or, at least, in a space with dimension less than 9. This system may therefore be viewed as a good model to investigate high-dimensional dynamics with tools used in the analysis of 3D models.

The 9D model provides a good opportunity to study how a high-dimensional system evolves when a control parameter is varied and what kind of departure from 3D systems may be observed (see section 3.3). This route to chaos is illustrated with two plane projections (figures 2 and 3) spanned by C_6–C_7 and C_6–C_9, respectively. In the range $r \in [14.10, 14.22]$, the period-doubling cascade is easily identified and does not seem to depend on the plane projections used. When the Rayleigh number is increased beyond 14.22, it becomes clear that differences in these representations of the dynamics may be
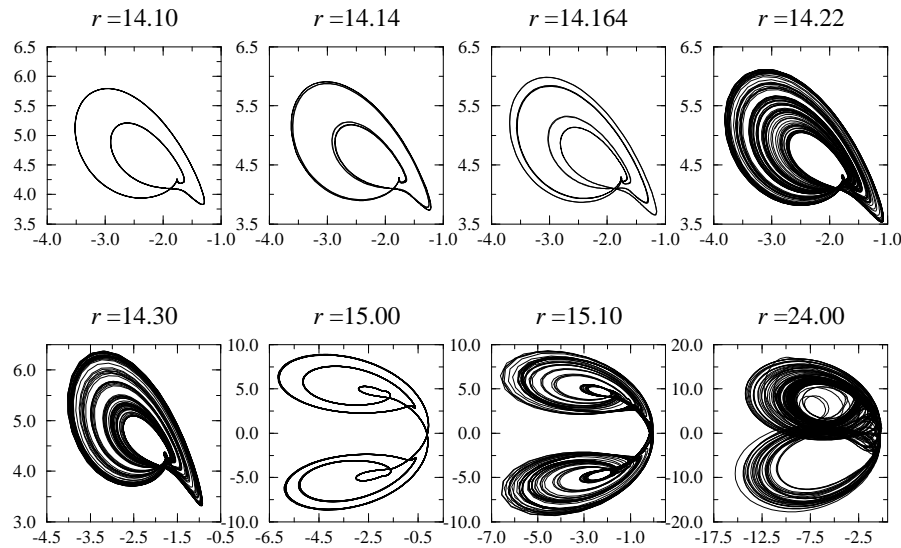
Figure 3. Phase space projections of the 9D attractor on the C_6–C_9 plane for $\sigma = 0.5$ and increasing r. The numerical integration is performed with the same conditions as in figure 2.
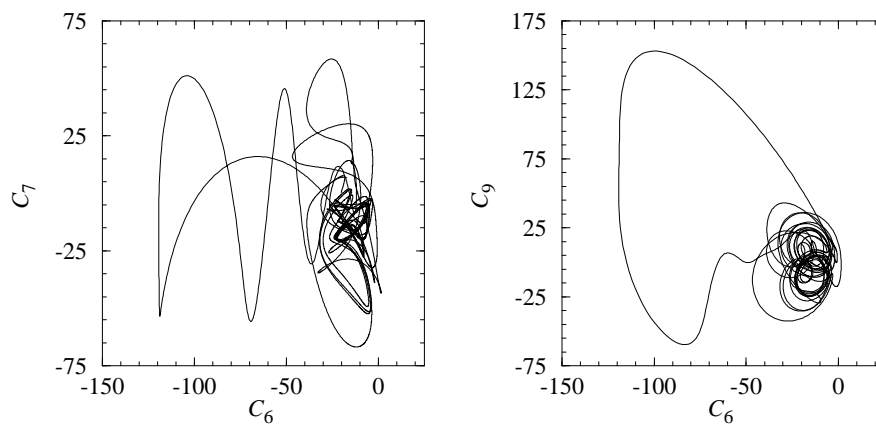

Figure 4. Two plane projections of the attractor generated by the 9D Lorenz system for $\sigma = 0.5$ and $r = 45.0$. The asymptotic behaviour is characterized by two positive Lyapunov exponents and is therefore identified as being hyperchaotic.

exhibited depending on the plane projection used. For instance, for $r = 14.30$, a double leaf attractor is observed in the C_6–C_7 plane projection (figure 2) while a simple attractor is found in the C_6–C_9 plane projection (figure 3). Such departure may arise from the symmetry properties of the 9D Lorenz model. Different dynamical variables may therefore provide different kinds of representation of the dynamics. This is clear when r is greater than 43.3, for which two Lyapunov exponents are found to be positive, leading to a hyperchaotic behaviour (figure 4). The study of this phenomenon goes beyond the scope of this paper and will be addressed in future studies.

3.2. Topological analysis

The topological characterization is based on the relative organization of periodic orbits embedded within the attractor. Such periodic orbits are viewed as knots and the way in which they are knotted and linked is characteristic of the dynamics studied. Unfortunately, in 4D spaces, all knots are trivial, i.e. isotopic to the circle S^1, and unlinked. Nevertheless, an attempt to characterize the rigid structure of the flow has recently been proposed by Mindlin and Solari [29] by using the organization of the surfaces associated with the local invariant manifolds of the orbits. Such a procedure is hopeful although not yet sufficiently developed to be directly used to validate models. Consequently, we prefer to limit ourselves to the use of common topological characterization by working in a sub-3D space in which we will investigate the dynamics. Rather than working in a space spanned by three variables C_i of the original system, we prefer to investigate the dynamics by working in a space spanned by one dynamical variable C_i and its successive time derivatives which is usually done when only a scalar time series is available [2, 3]. We designate this representation by the *differential embedding*.

We arbitrarily make C_5 the 'recorded' time series for $r = 14.22$. The working space is therefore spanned by

$$\begin{cases} X(t) = C_5(t) \\ Y(t) = \dot{C}_5(t) \\ Z(t) = \ddot{C}_5(t). \end{cases}$$

In the reconstructed space, the asymptotic motion describes an attractor as displayed in figure 5(a). The first-return map of a Poincaré section is computed and found to be a unimodal map whose maximum is differentiable as expected after a period-doubling cascade (figure 6(a)). One may remark that this unimodal map, constituted by two monotonic branches, presents a decreasing branch which is split into two parts. It is a characteristic signature of the dynamics which will be discussed in section 3.3. The critical point X_C allows one to define a generating partition of the attractor in different regions. This means that the attractor may be viewed as constituted by two strips whose topological properties are different, each one being associated with a monotonic branch of the first-return map. The increasing branch is roughly associated with a strip located in the inner part of the attractor without a half-turn while the second strip, corresponding to the decreasing branch, is located in the outer part of the attractor and presents a negative π-twist (i.e. a negative half-turn). A sketch of these two strips is displayed in figure 7. Following a pioneering paper by Birman and Williams [30], it has been shown [11, 13, 31] that a template may synthetize the topological properties of an attractor embedded in a 3D phase space.

Usually, a unimodal map induces a template consisting of two strips [12, 13, 26, 32]. Following a standard insertion convention [31], strips must be re-injected into the bottom band from back to front and from left to right. This convention allows an unambiguous description of the template by defining a linking matrix whose diagonal elements M_{ii} are equal to the number of π-twists of the ith strip, and off-diagonal elements M_{ij} ($i \neq j$) are given by the algebraic number of intersections between the ith and jth strips.

Each strip may be labelled: 0 designates the strip associated with the increasing branch while 1 is associated with the strip corresponding to the decreasing branch. In this way, chaotic trajectories and periodic orbits are encoded by a string of 0's and 1's. The kneading sequence [9] is found to be encoded by $(\overline{10110})$. Thus we have defined a symbolic dynamics. For details on symbolic dynamics, the reader may consult [9, 10, 25]. The template is validated by counting linking numbers between pairs of periodic orbits projected in a regular
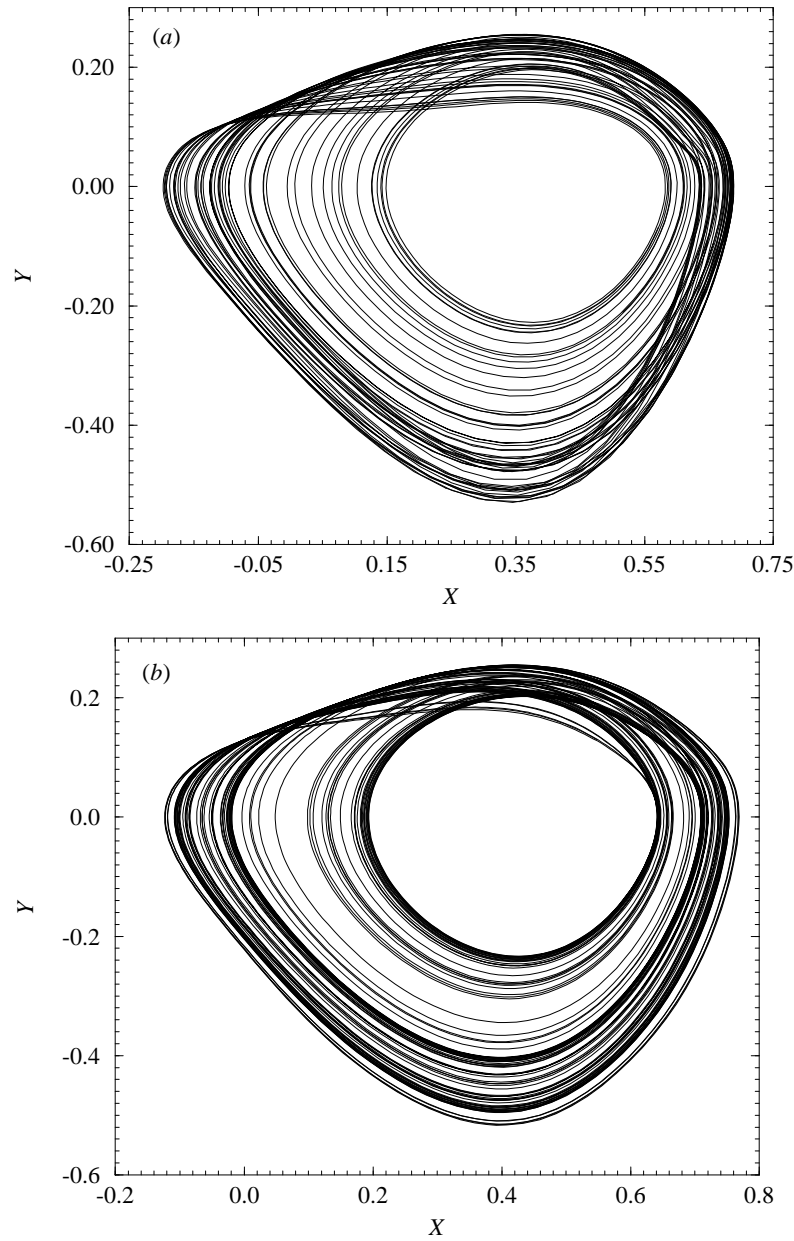
Figure 5. Plane projections of the C_5-attractors (r=14.22). (a) Differential embedding, (b) 3D reconstructed model, (c) 4D reconstructed model.

plane as exemplified in figure 8(a) and by comparing them with the template predictions [13, 25, 33]. The linking number is defined as half of the algebraic sum of the oriented
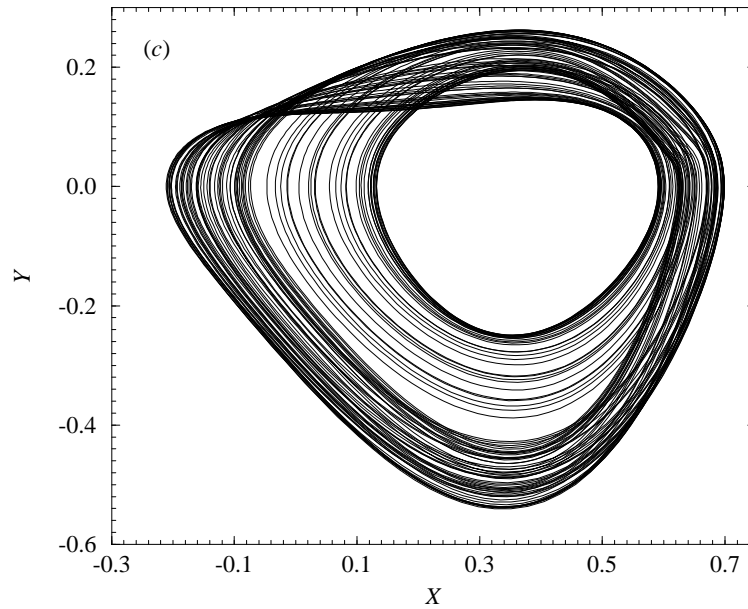
Figure 5. (Continued)

crossings according to

$$+1 \qquad -1 \quad .$$

Only by inspecting the three linking numbers

$$\begin{cases} lk(10, 1) = 0 \\ lk(1011, 1) = -1 \\ lk(1011, 10) = -2 \end{cases}$$

did we find that a 2×2 linking matrix cannot be defined to predict all of them. Therefore a template cannot be built to synthetize the topological properties of the dynamics. In other words, the C_5-attractor cannot be embedded in a 3D phase space. Consequently, a higher-dimensional phase space is required. The value of the embedding dimension will be determined by using a global vector field reconstruction technique.

3.3. Global vector field reconstruction

A way to investigate a dynamical system may be the use of a global vector field reconstruction technique, i.e. a set of ODEs which models the dynamical behaviour is obtained starting from a given scalar time series. This is of particular interest in our case since we will prove that the topological structure of the 3D model reconstructed from a C_5 time series is not compatible with the topology of the C_5-attractor. On the contrary, a 4D model will be found to be compatible with the C_5-attractor.
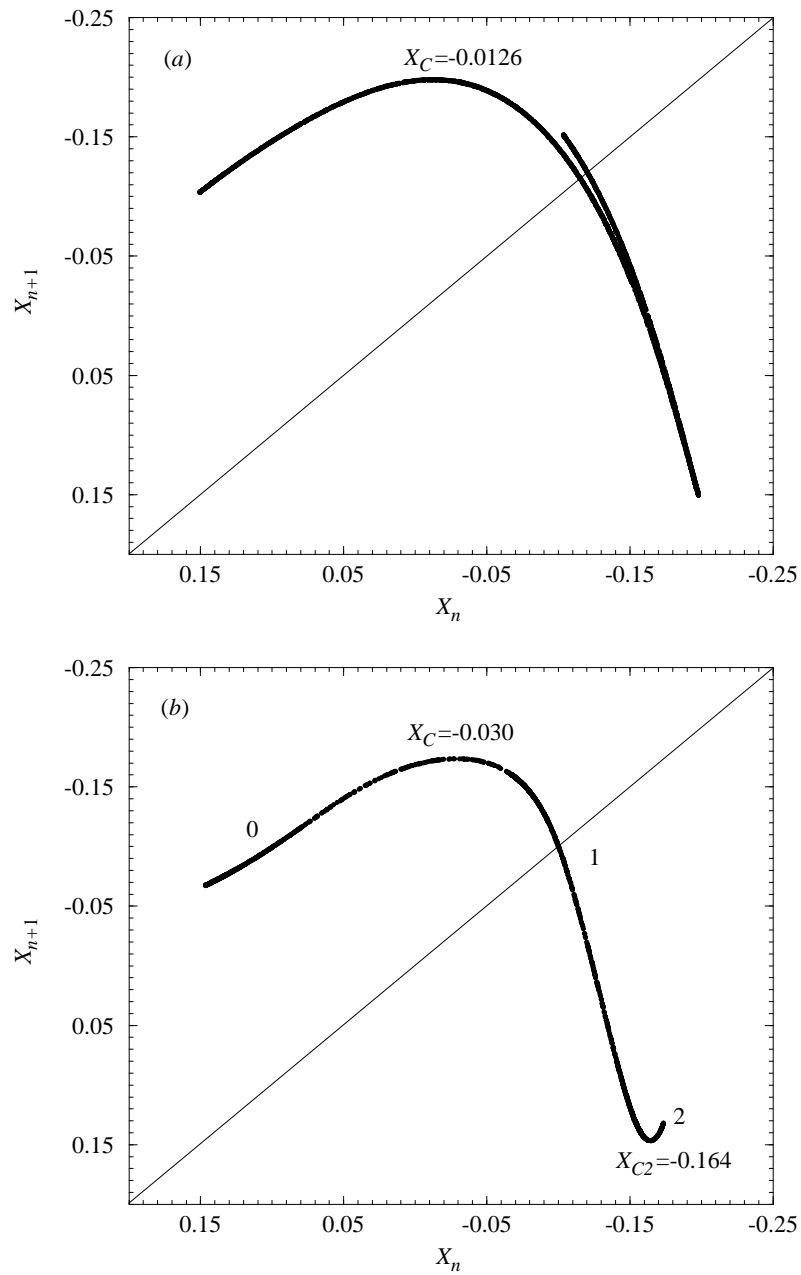
Figure 6. First-return maps of a Poincaré section for the C_5-attractors. (*a*) Differential embedding, (*b*) 3D reconstructed model, (*c*) 4D reconstructed model.

Our main goal is to reconstruct a d_E-dimensional vector field generating dynamics topologically equivalent to the original dynamics generated by the 9D Lorenz model. The reconstructed model involves the C_5-time series and its $(d_E - 1)$ successive derivatives as
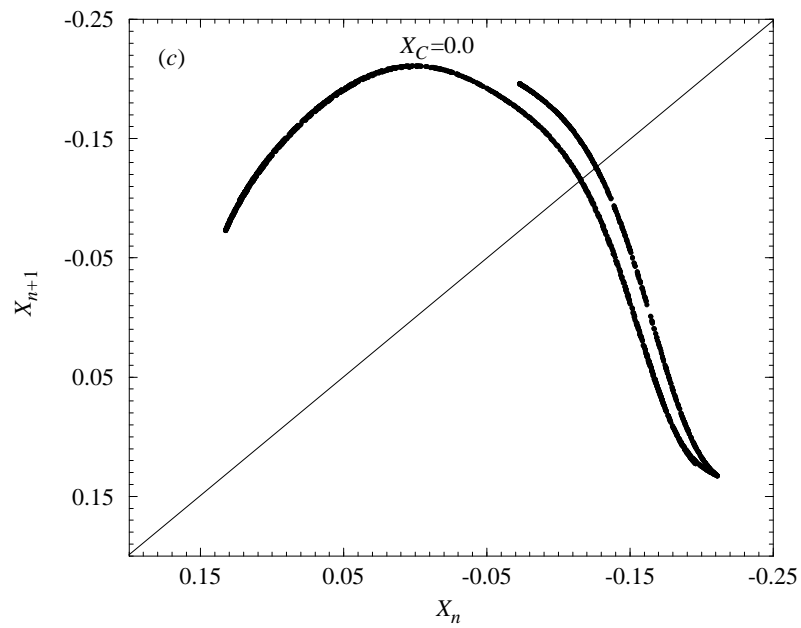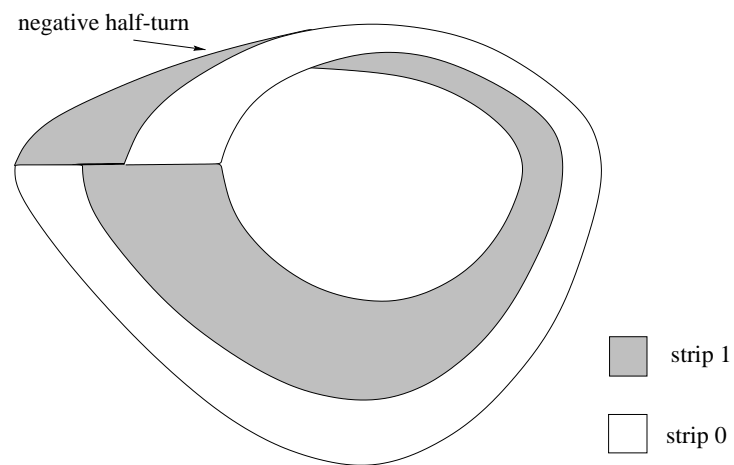
Figure 6. (Continued)

Figure 7. Sketch of the two main strips constituting the 3D reconstructed model starting from the C_5-time series ($r=14.22$).

dynamical variables. It reads as:

$$\begin{cases} \dot{X}_1 = X_2 \\ \dot{X}_2 = X_3 \\ \vdots \\ \dot{X}_{d_{\mathrm{E}}} = F(X_1, X_2, \ldots, X_{d_{\mathrm{E}}}) \end{cases}$$

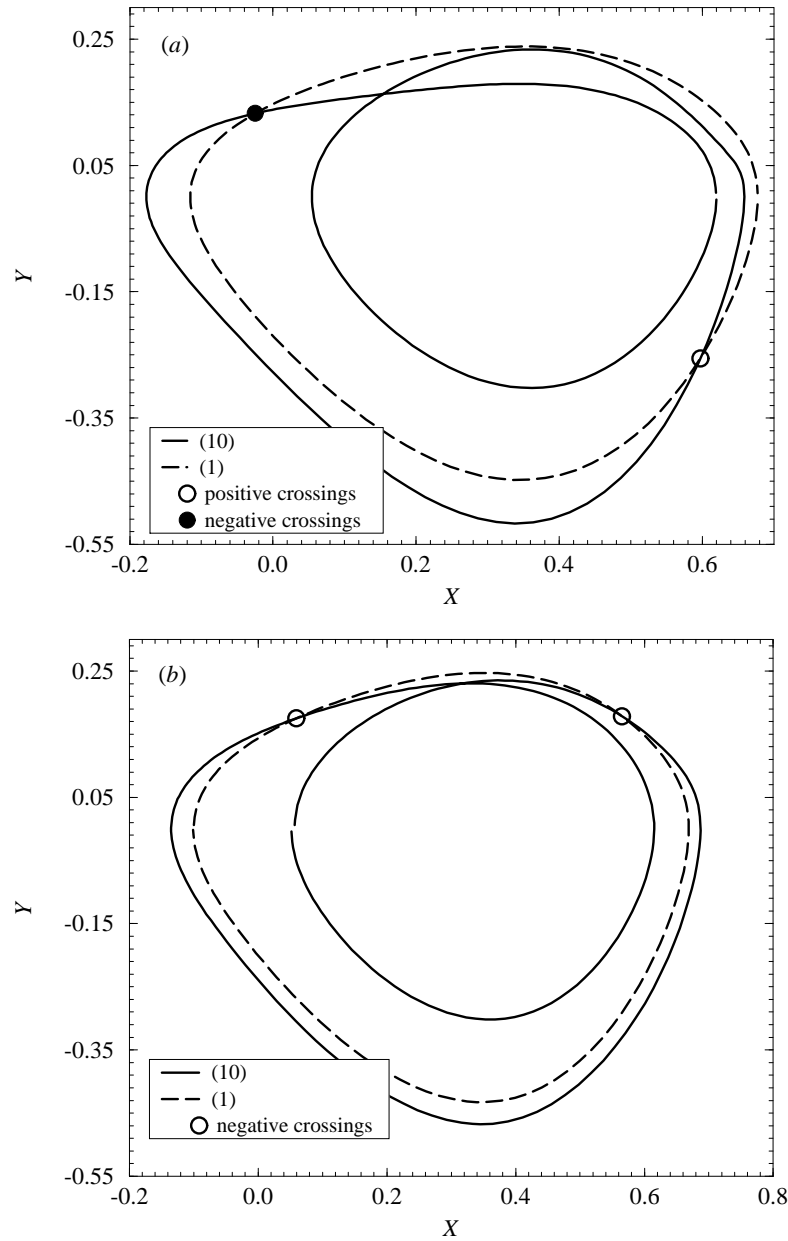where F is a function to be estimated. The function F is expressed in terms of monomials

Figure 8. Plane projections of the pairs of periodic orbits extracted from the C_5-attractors encoded by (10) and (1), respectively. (*a*) Differential embedding, (*b*) 3D reconstructed model, (*c*) 4D reconstructed model.

$P^n = X_1^{k_1} X_2^{k_2} \ldots X_{d_E}^{k_{d_E}}$ where a relationship between d_E-tuplets $(k_1, k_2, \ldots, k_{d_E})$ and integers n has been extended from the relationship introduced in [34]. The approximation $\tilde{F}$ is obtained by using a Fourier expansion on a multivariate polynomial basis on nets [34]. The algorithm requires the definition of reconstruction parameters which are (i) d_E, the embedding dimension, (ii) N_q, the number of vectors $(X_{1,i}, X_{2,i}, \ldots, X_{d_E,i}, \dot{X}_{d_E,i})$
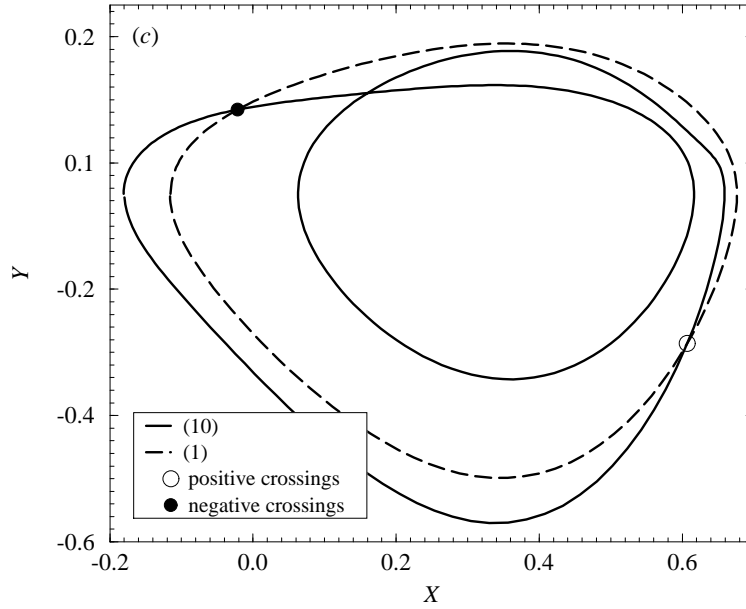
Figure 8. (Continued)

$(i \in [1, N_q])$ on the nets with i as a time index, (iii) Δt, the timestep between two successive vectors which may be expressed as the number of vectors, N_s, sampled per pseudoperiod, (iv) N_p, the number of retained polynomials and (v) τ_W, the window size on which the derivatives are estimated by deriving a polynomial fitted with a singular value decomposition technique. The reconstruction parameters are found with the help of an error function

$$E_r = \frac{\sum_{i=1}^{N_q} |\dot{X}_{d_E,i} - F(X_1, X_2, \ldots, X_{d_E})|}{\sum_{i=1}^{N_q} |\dot{X}_{d_E,i}|}.$$

We obtain a model with reconstruction parameters:

$$\begin{cases} d_E = 3 \\ N_q = 67 \\ N_s = 13 \\ N_p = 35 \\ \tau_W = 7\delta t = 7 \cdot 0.05. \end{cases}$$

By integrating this 3D reconstructed model, we obtain the phase portrait displayed in figure 5(*b*). It may be favourably compared with the plane projection of the C_5-attractor (figure 5(*a*)). A first-return map to a Poincaré section (figure 6(*b*)) is found to be mainly constituted by two monotonic branches separated by a differentiable maximum as observed on the first-return map computed for the C_5-attractor (figure 6(*a*)). One may remark that a third branch appears, but the kneading sequence remains encoded by $(\overline{101})$. No orbits with periods smaller than 8 are found to be encoded by symbolic sequences involving the symbol 2. The population of periodic orbits is therefore not very different from the one extracted from the C_5-attractor. Only two period-7 orbits and one period-3 orbit, which are not embedded within the C_5-attractor, have been extracted from the attractor generated by the 3D model. By counting linking numbers between pairs of periodic orbits embedded
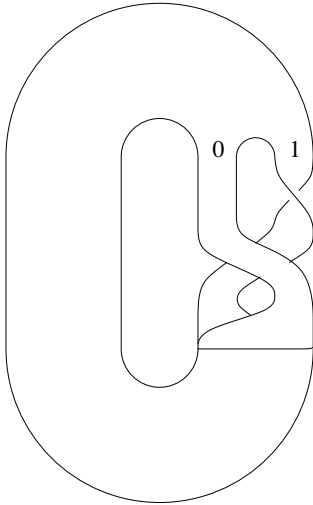
Figure 9. Template of the attractor generated by the 3D reconstructed model starting from the C_5 time series.

within the reconstructed attractor, we find that they are easily predicted by the template (figure 9) defined by the linking matrix

$$M \equiv \begin{bmatrix} 0 & -1 \\ -1 & -1 \end{bmatrix}.$$

The reconstructed model generates therefore an attractor whose topological properties can be synthetized by a template; for instance, the pair of periodic orbits encoded by (10) and (1) (figure 8(*b*)) whose linking numbers are easily predicted by the template (figure 9). One may also remark that this linking number is different from the one counted for the C_5-attractor. The topological properties are therefore different, and the 3D model cannot be validated.

By reconstructing a 3D model, the structure of the dynamics is constrained to be compatible with 3D dynamics which is well characterized by a template. Such results demonstrate that the embedding dimension must be greater than 3 since topological properties of the C_5-attractor cannot be described by a template which constitutes a signature of a 3D dynamics. Nevertheless, such a model whose dynamics is not so far from the one underlying the C_5-attractor suggests that the embedding dimension d_E is close to 3.

We therefore attempt a 4D model with reconstruction parameters:

$$\begin{cases} d_E = 4 \\ N_q = 334 \\ N_s = 10 \\ N_p = 70 \\ \tau_W = 7\delta t = 7 \cdot 0.05. \end{cases}$$

A plane projection of the attractor generated by integrating this 4D model is displayed in figure 5(*c*). Once again, a visual inspection of this projection may be favourably compared with figure 5(*a*). A first-return map to a Poincaré section (figure 6(*c*)) is found to be constituted by an increasing branch and a decreasing branch which is split into two segments as observed for the C_5-attractor (figure 6(*a*)). The kneading sequence of the 4D reconstructed attractor is encoded by $(\overline{101})$, i.e. the population of periodic orbits is slightly different from the population of the C_5-attractor. All linking numbers counted on

plane projections of periodic orbits extracted from the 4D reconstructed attractor are in agreement with those counted from the C_5-attractor as exemplified by the plane projection of the pair (10, 1) (figure 8(*c*)). The 4D model is therefore validated. One may note that only a topological characterization, although working in a 3D subspace providing the same 3D projection of the 4D phase space, allows one to distinguish two classes between these three models. The first class is constituted by the C_5-attractor and the 4D reconstructed attractor whose topological properties cannot be synthetized by a template. The second class is constituted by the 3D reconstructed attractor whose topological properties are well described by a template. The 4D model confirms that the smallest embedding dimension is equal to 4.

4. Conclusion

By applying a triple Fourier series ansatz up to second order, we obtained a system of nine nonlinear ODEs. We showed that this model presents a period-doubling cascade for a given set of control parameter values. Since this route to chaos defines a universal class of dynamics, it is usually expected that chaotic behaviour beyond this cascade corresponds to a horseshoe dynamics. By using a global vector field reconstruction technique, we argued that the embedding dimension of the attractor generated by the 9D Lorenz model is equal to 4. This 9D Lorenz model is therefore a very interesting model for investigating chaotic dynamics in a phase space with a dimension greater than 3. Indeed, it is a very helpful model in developing new tools characterizing high-dimensional chaos as exemplified by the case of the topological characterization which is not effective for a space whose dimension is greater than 3. Although a topological characterization is not rigorously available in a space with a dimension greater than 3 it may be useful to validate higher-dimensional models by working in a 3D subspace, i.e. in a projection of the whole phase space.

The interest of this model arises from the fact that it generates a chaotic behaviour beyond a period-doubling cascade and, consequently, the simplest 4D chaotic attractor which may be expected. In addition, this model presents an interesting bifurcation diagram starting from a period-doubling cascade and evolving up to a hyperchaotic behaviour which is yet to be investigated.

Acknowledgments

References

[1] Lorenz E N 1963 Deterministic nonperiodic flow *J. Atmos. Sci.* **20** 130–41
[2] Packard N H, Crutchfield J P, Farmer J D and Shaw R S 1980 Geometry from a time series *Phys. Rev. Lett.* **45** 712–16
[3] Takens F 1981 Detecting strange attractors in turbulence *Dynamical Systems and Turbulence (Lecture Notes in Mathematics 898)* ed D A Rand and L S Young (Berlin: Springer) pp 366–81
[4] Grassberger P and Proccacia I 1983 Measuring the strangeness of strange attractors *Physica* **9D** 189–208
[5] Eckmann J P, Oliffson S, Ruelle D and Ciliberto S 1986 Lyapunov exponents from time series *Phys. Rev.* A **34** 4971–9

[6] Abarbanel H D I, Brown R, Sidorowich J J and Tsimring L Sh 1993 The analysis of observed chaotic data in physical systems *Rev. Mod. Phys.* **65** 1331–88

[7] Abarbanel H D I 1995 Analysing and utilizing time series observations from chaotic systems *Nonlinearity and Chaos Engineering Dynamics* ed J M T Thompson and S R Bishop (New York: Wiley) pp 379–91

[8] Metropolis N, Stein M L and Stein P R 1973 On finite limit sets for transformations on the unit interval *J. Comb. Theor.* A **15** 25–44

[9] Collet P and Eckmann J P 1980 *Iterated Maps on the Interval as Dynamical Systems (Progress in Physics)* ed A Jaffe and D Ruelle (Boston, MA: Birkhäuser)

[10] Hall T 1994 The creation of horseshoes *Nonlinearity* **7** 861–924

[11] Mindlin G B, Hou X J, Solari H G, Gilmore R and Tufillaro N B 1990 Classification of strange attractors by integers *Phys. Rev. Lett.* **64** 2350–3

[12] Mindlin G B, Solari H G, Natiello M A, Gilmore R and Hou X J 1991 Topological analysis of chaotic time series data from the Belousov–Zhabotinski reaction *J. Nonlin. Sci.* **1** 147–73

[13] Tufillaro N B, Abbott T and Reilly J 1992 *An Experimental Approach to Nonlinear Dynamics and Chaos* (New York: Addison-Wesley)

[14] Rössler O E 1979 An equation for hyperchaos *Phys. Lett.* **71A** 155–7

[15] Rössler O E 1976 An equation for continuous chaos *Phys. Lett.* **57A** 397–8

[16] Cordon R P and Velarde M G 1975 On the (nonlinear) foundations of Boussinesq approximation applicable to a thin layer of fluid *J. Physique* **36** 591–601

[17] Normand C and Pomeau Y 1977 Convective instability: a physicist's approach *Rev. Mod. Phys.* **49** 581–624

[18] Palm E 1975 Nonlinear thermal convection *Annu. Rev. Fluid Mech.* **7** 39–61

[19] Lord Rayleigh 1916 On convection currents in a horizontal layer of fluid when the higher temperature is on the under side *Phil. Mag.* **32** 529–46

[20] Chandrasekhar S 1961 *Hydrodynamic and Hydromagnetic Stability* (Oxford: Clarendon)

[21] Koschmieder E L 1993 *Bénard Cells and Taylor Vortices* (Cambridge: Cambridge University Press)

[22] Benettin G, Galgani L, Giorgilli A and Strelcyn J M 1980 Lyapunov characteristic exponents for smooth dynamical systems and for Hamiltonian systems: a method for computing all of them *Meccanica* **15** 9–30

[23] Feigenbaum M J 1978 Quantitative universality for a class of nonlinear transformation *J. Stat. Phys.* **19** 25–52

[24] Coullet P and Tresser C 1978 Itérations d'endomorphismes et groupe de renormalisation *J. Physique* **8** C5–25

[25] Letellier C, Dutertre P and Maheu B 1995 Unstable periodic orbits and templates of the Rössler system: toward a systematic topological characterization *Chaos* **5** 271–82

[26] Letellier C, Le Sceller L, Dutertre P, Gouesbet G, Fei Z and Hudson J L 1995 Topological characterization and global vector field reconstruction from an experimental electrochemical system *J. Phys. Chem.* **99** 7016–27

[27] Franceschini V and Tebaldi C 1979 Sequences of infinites bifurcations and turbulence in five-mode truncation of the Navier–Stokes equations *J. Stat. Phys.* **21** 707

[28] Press W H, Flannery B P, Teukolsky S A and Vetterling W T 1995 *Numerical Recipes in C* (Cambridge: Cambridge University Press)

[29] Mindlin G B and Solari H G 1997 Tori and Klein bottles in four-dimensional chaotic flows *Physica* **102D** 177–86

[30] Birman J S and Williams R F 1983 Knotted periodic orbits in dynamical systems: Lorenz's equations *Topology* **22** 47–82

[31] Melvin P and Tufillaro N B 1991 Templates and framed braids *Phys. Rev.* A **44** 3419–22

[32] Tufillaro N B, Wyckoff P, Brown R, Schreiber T and Molteno T 1995 Topological time series analysis of a string experiment and its synchronized model *Phys. Rev.* E **51** 164–74

[33] Le Sceller L, Letellier C and Gouesbet G 1994 Algebraic evaluation of linking numbers of unstable periodic orbits in chaotic attractors *Phys. Rev.* E **49** 4693–5

[34] Gouesbet G and Letellier C 1994 Global vector field reconstruction by using a multivariate polynomial L_2-approximation on nets *Phys. Rev.* E **49** 4955–72